Supplementary Information for

Ordered Boron Phosphorus Codoped Graphene Realizing Widely Tunable Quasi Dirac-cone Gap

L.-B. Meng, S. Ni, Z. M. Zhang, S. K. He, and W. M. Zhou

1. Computational details

1.1. DFT calculation.— The first-principles calculations were conducted on the basis of density functional theory (DFT) with the projector augmented wave pseudopotential [1] method as implemented in the Vienna Ab initio Simulation Package (VASP) [2]. The electron exchange-correlation potential was treated by the Perdew-Burke-Ernzerhof (PBE) functional [3] in structural optimization and energy calculations. A 600 eV energy cutoff was adopted and the Brillouin zone was sampled with a 15 ×15 ×1 Monkhorst-Pack (MP) [4] *k*-point grid for geometry optimization. The energy threshold was set to 10^{-6} eV, and the atomic position was fully relaxed until the maximum force on each atom was less than 10^{-4} eV/Å. As the semilocal functional underestimates the band gap for most of the insulators, to determine the gap reliably, the band structure was computed by the reputed hybrid Heyd-Scuseria-Ernzerhof (HSE06) functional [5] with a sufficient 11 ×11 ×1 MP *k*-point (gap convergence within relative error of < 0.6%). Phonon calculations by the finite displacement method with 3 ×3 × 1 supercell implemented in the PHONOPY code [6] were adopted to examine the dynamic stability. The *ab initio* molecular dynamics (AIMD) simulations were carried out under constant temperature and volume (NVT) with the temperature controlled by a Nosé-Hoover thermostat [7] to insure the thermal stability. The initial configurations of the alloy with a 4 × 4 ×1 supercell were annealed at respective temperatures of 300—2400 K lasting for 8 picosecond (ps) with a time step of 2 femtosecond (fs). The Hirshfeld charge popular analyses were performed by the CASETEP software [8].

1.2. PSO search.— The swarm-intelligence global searches for the lowest-energy structures of the alloy were performed with the particle-swarm optimization (PSO) method as implemented in the well-established Crystal structure AnaLYsis by Particle Swarm Optimization (CALYPSO) program [9]. In the PSO calculations, the number of formula units per simulation cell was set as 1, 2, and 3, and both the population size and the number of generation were set to 30. The structure relaxations during the PSO simulation were performed using the PBE functional as implemented in VASP.

1.3. Carrier mobility.— The carrier mobility (μ) for a 2D material in the DP theory can be expressed as an acoustic-phonon-limited format [10,11]:

$$\mu = \frac{2e\hbar^3 C}{3k_B T(m^*)^2 {E_1}^2}$$

where T is the temperature and m^* is the effective mass of the carrier along the transport direction; $E_1 = \Delta v/(\Delta l/l_0)$ is the DP constant, where Δv represents the shift of band edges under proper cell compression and dilatation, l_0 the lattice constant in the transport direction, and Δl its deformation; $C = (\partial^2 E/\partial\delta^2)/S_0$ is the elastic modulus, where E is the total energy of the cell and δ the applied strain while S_0 is the area of the cell.

1.4. Topological Z_2 invariant.— The topological Z_2 invariant was calculated by the HSE06 functional in conjunction with the SOC effect via the auxiliary WannierTools code [12], in which the topological number Z_2 derived by the calculations of the Wilson loop (Wannier charge center) for six time reversal invariant planes. The p_z orbitals of B, C and P atoms were selected as the initial projectors for the Wannier wave functions.

2. Supplemental figures, tables and notes

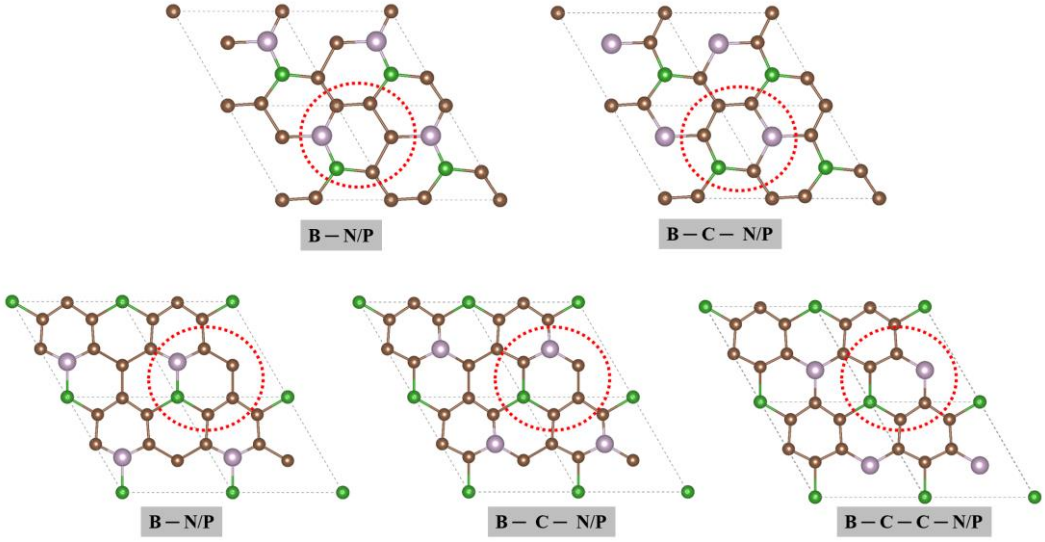

Figure S1. Candidate structures of pairing IIIA B and VA N/P atoms codoped honeycomb lattice in the initio inspection. They are constructed from the 2:1-C_2Si-type [13] and 3:1-$C_3B(P)$-type [14,15] structures with different combinations of the B and N/P bondings.

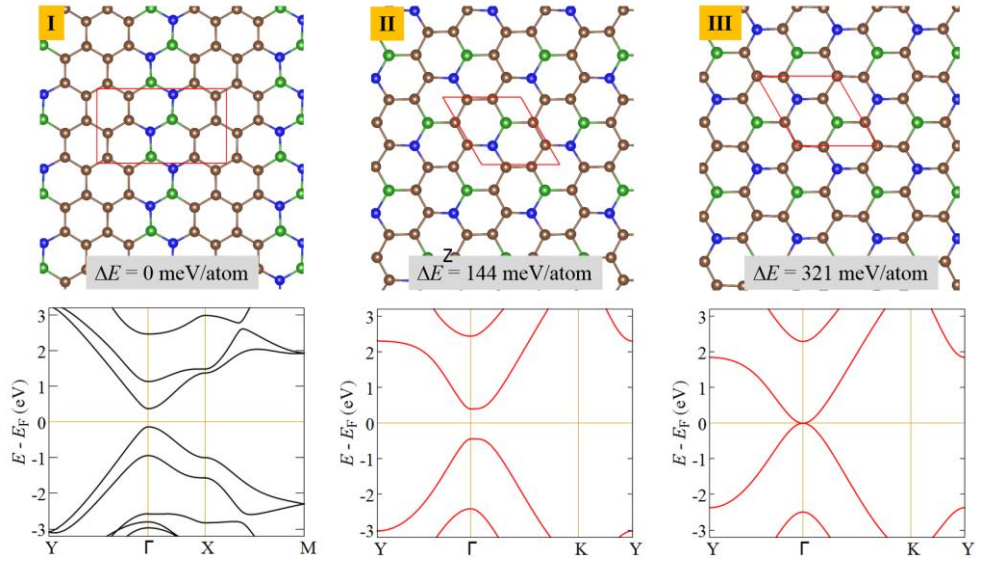

Figure S2. Low-energy isomers of C_4BN by PSO search and corresponding PBE (black) and HSE06 (red) band structures. Energies are relative to the minimal-energy structure. Structure I is the minimal energy of PSO search. Structures II and III are ones in the initio inspection.

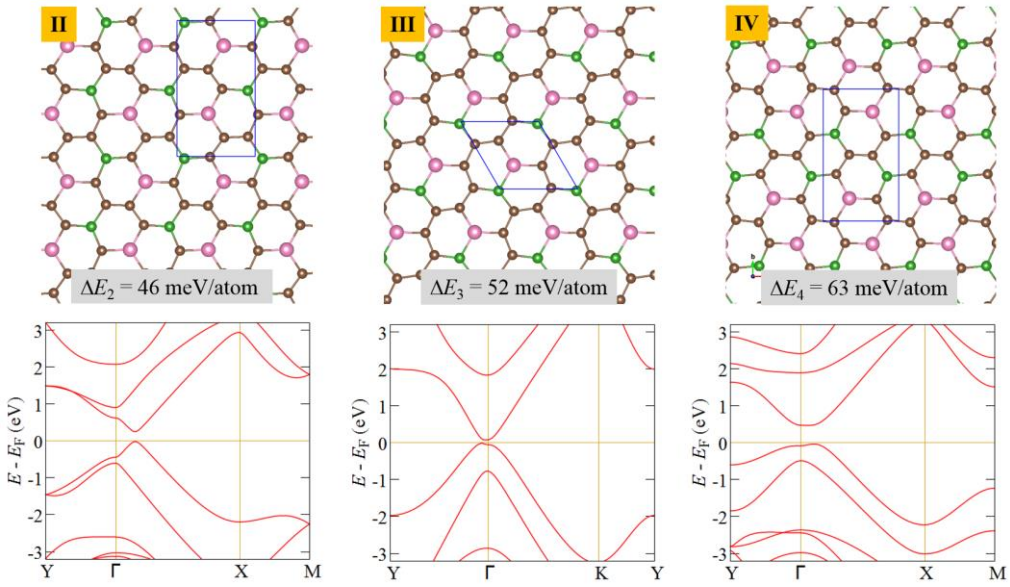

Figure S3. Low-energy isomers of C_4BP by PSO search and corresponding HSE06 band structures. Energies are relative to the minimal-energy structure. Structure discussed in the text, which is the minimal energy corresponding to $\Delta E_1 = 0$ meV/atom, is not shown here. Structure discussed in the text and III are ones in the initio inspection.

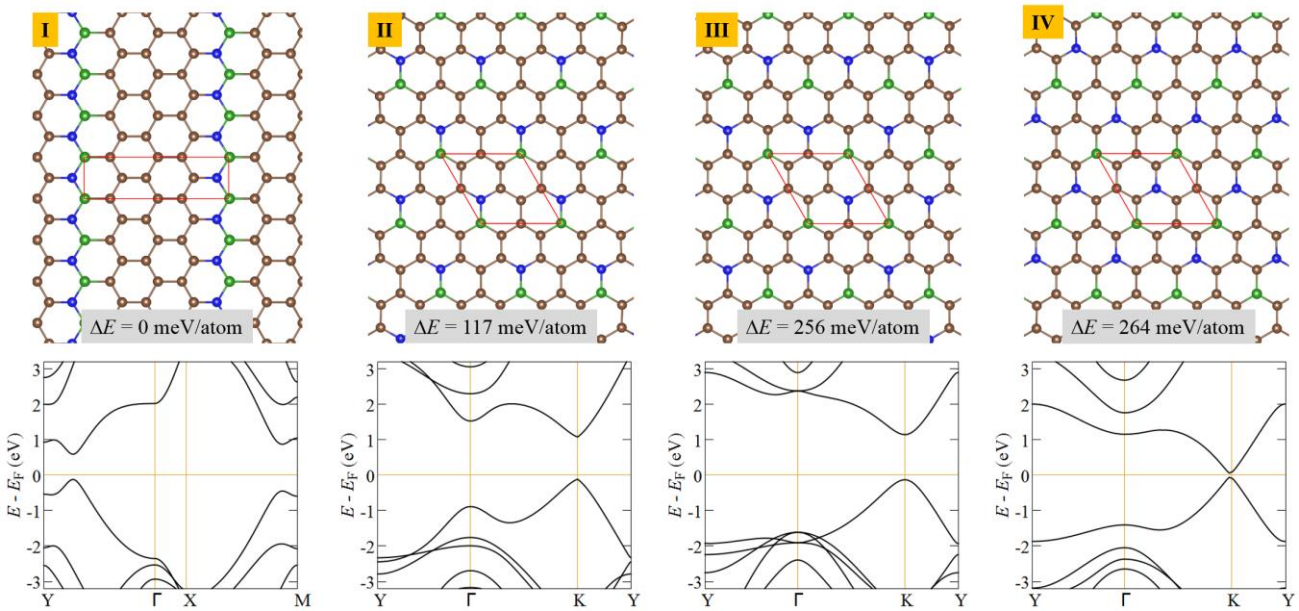

Figure S4. Low-energy isomers of C_6BN by PSO search and corresponding PBE band structures. Energies are relative to the minimal-energy structure. Structure I is the minimal energy of PSO search. Structures II, III and IV are ones in the initio inspection.

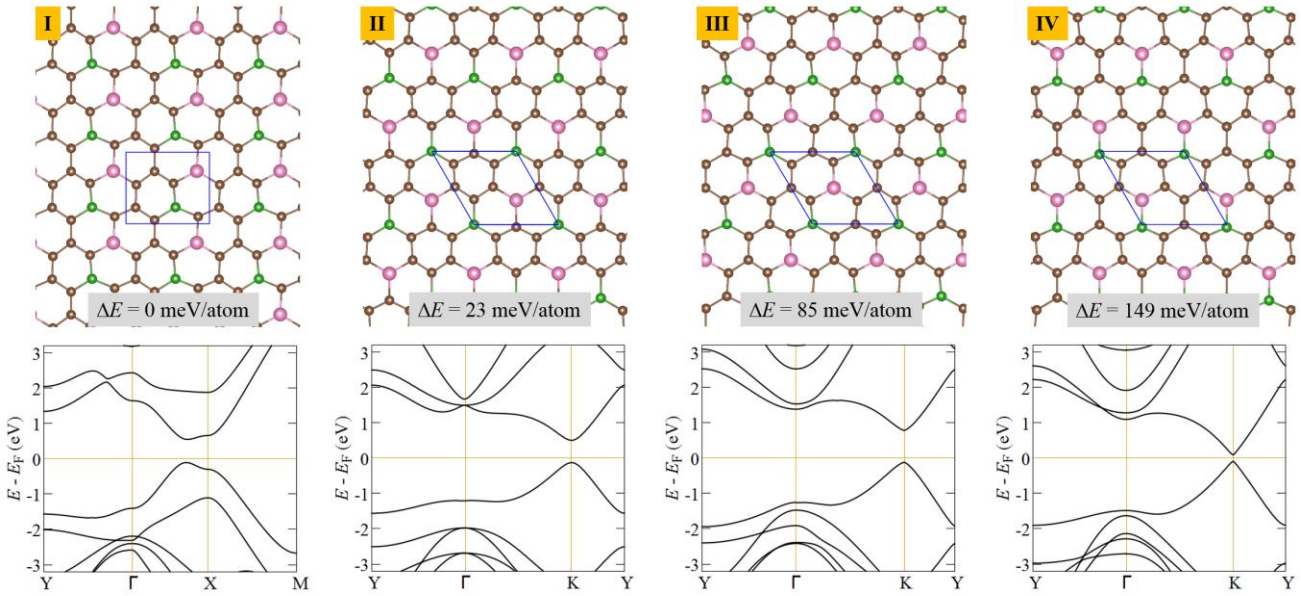

Figure S5. Low-energy isomers of C_6BP by PSO search and corresponding PBE band structures. Energies are relative to the minimal-energy structure. Structure I is the minimal energy of PSO search. Structures II, III and IV are ones in the initio inspection.

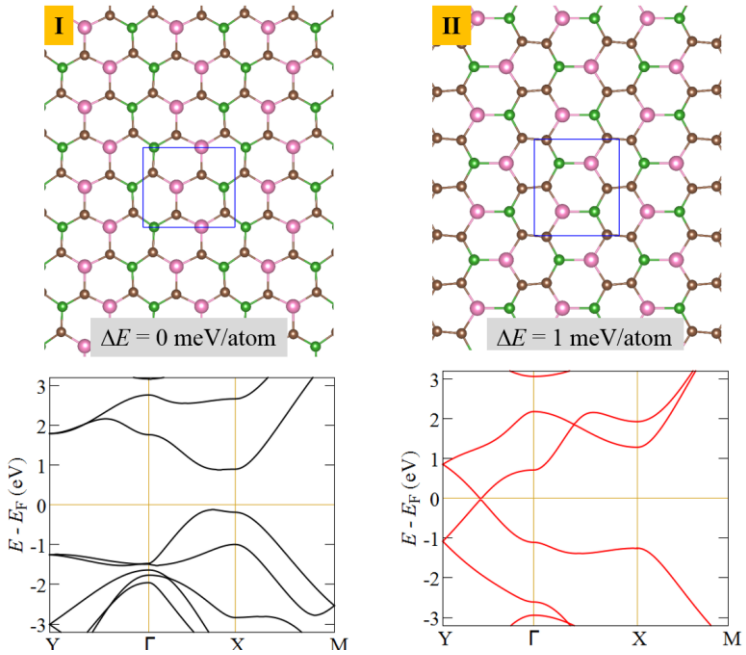

Figure S6. Low-energy isomers of C_2BP by PSO search and corresponding PBE (black) and HSE06 (red) band structures.

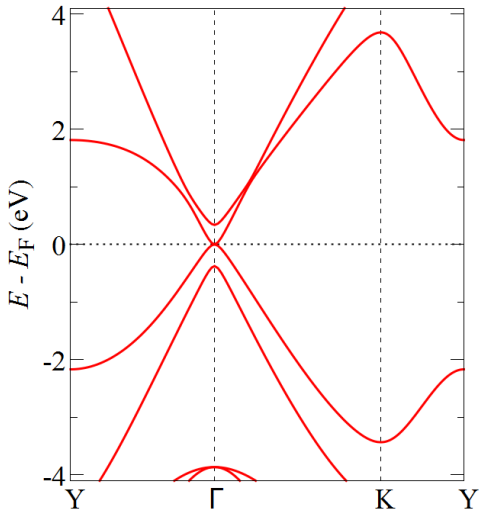

Figure S7. HSE06 band structure of the hypothetical $\sqrt{3} \times \sqrt{3}$ graphene with C atoms arranged in the geometrical parameters of C_4BP (C_{3h} point group).

It is a gapless semimetal with CBM and VBM contacting at Γ point. The pure broken spacial group symmetry from D_{6h} of pristine graphene to C_{3h} here does not induce a gap.

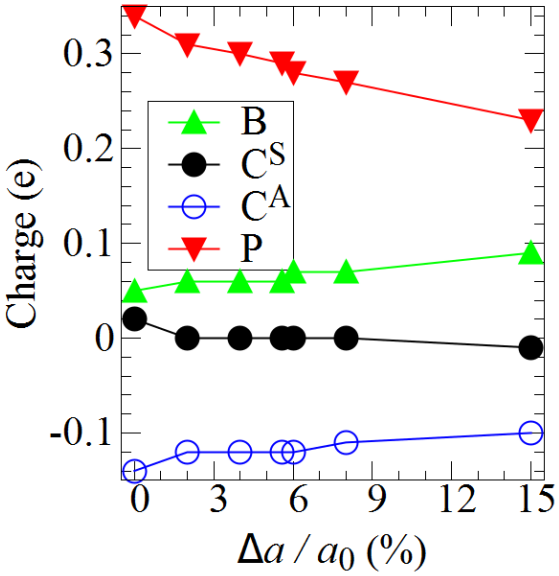

Figure S8. Calculated Hirshfeld charges of C_4BP under different tensile strains.

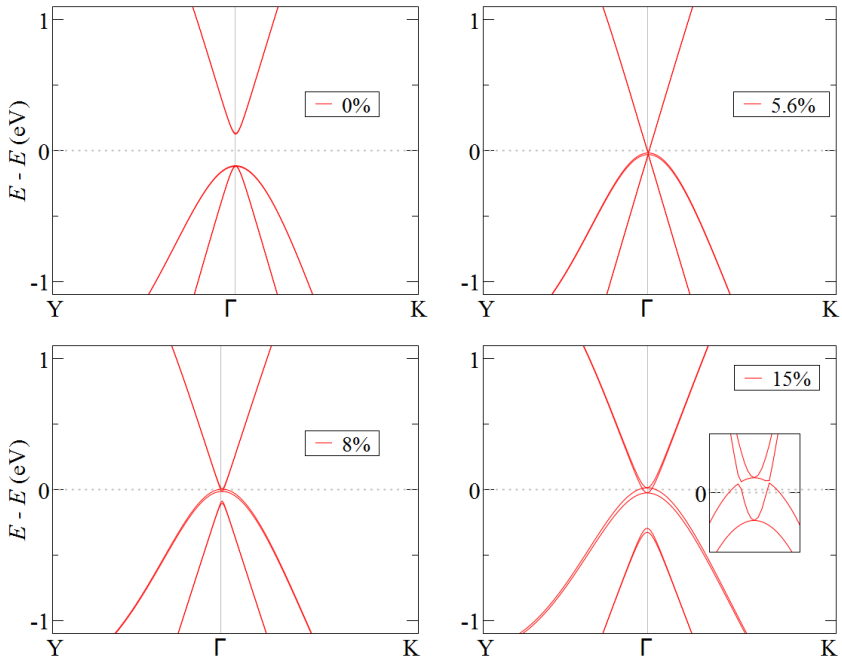

Figure S9. HSE06+SOC band structures of four representative tensile strains. The inset in the last one displays the local magnification for the gap.

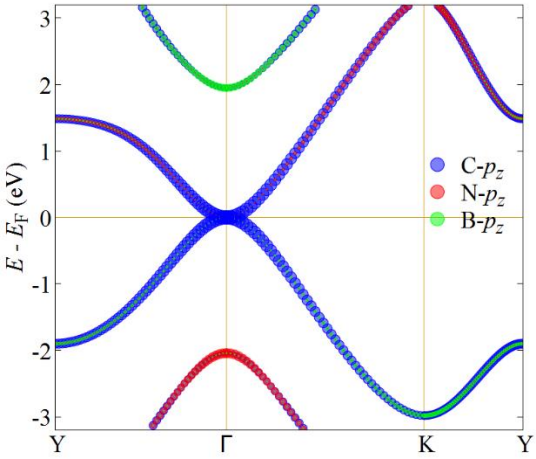

Figure S10. Orbital-resolved fat-band structure of C_4BN isomer III (Fig. S2, the counterpart of C_4BP in the text). The contribution of the *s*, p_x and p_y orbitals is negligible at the CBM and VBM and not shown.

The CBM and VBM are predominantly contributed by the C-p_z orbital in C_4BN here, while the N-p_z orbital is tiny. This is very different from that in C_4BP, where the P-p_z orbital has a considerable contribution for the CBM and VBM [Fig. 2(b)].

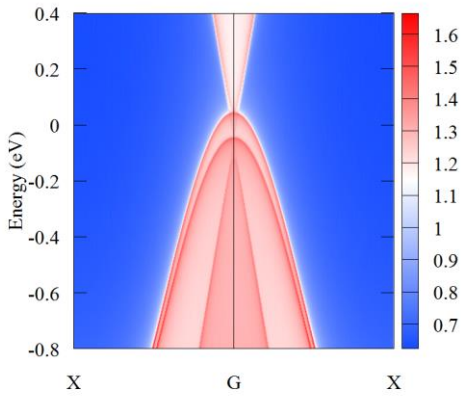

Figure S11. The calculated edge states of C_4BP monolayer for the strain of δ = 8%.

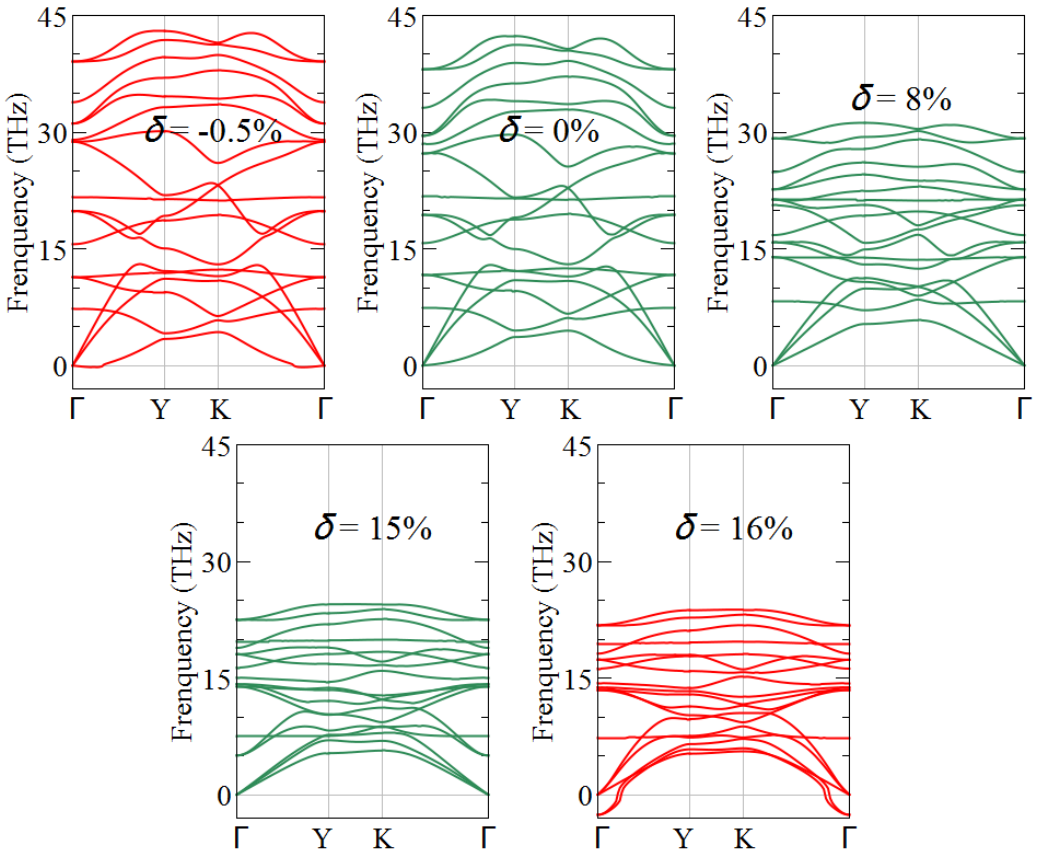

Figure S12. Phonon spectra of C_4BP along the high-symmetry points and axes under different biaxial tensile strains.

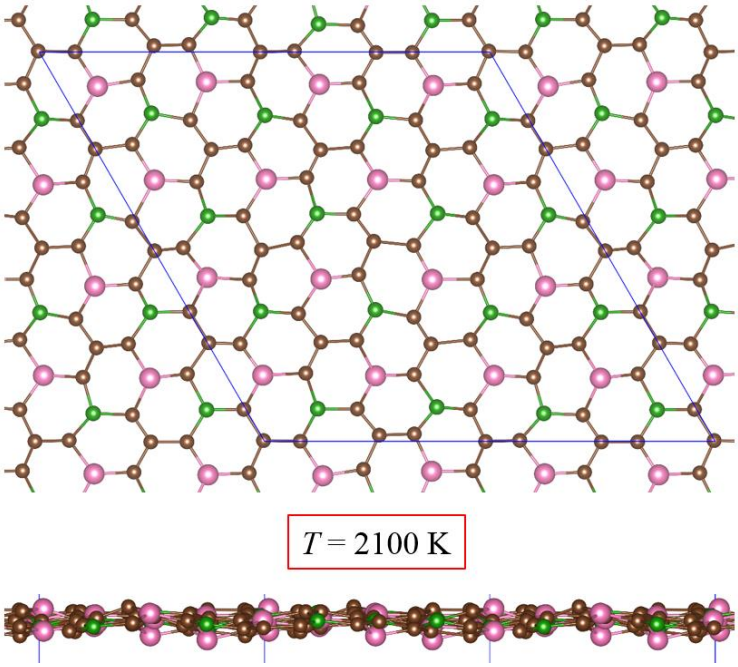

Figure S13. Structure snapshot for 8 ps AIMD simulations of C_4BP in 4 ×4 supercell at the temperature of 2100 K.

Table S1: Prediction of HSE06 bandgaps (meV) for different strains with/without the SOC effect.

Strains δ	0%	2.5%	5.6%	7%	8%	15%
Without SOC	247.2	128.1	0.0	0.0	0.0	0.0
With SOC	240.8	121.8	0.3	0.2	0.7	1.2

Table S2: Prediction of topological Z_2 invariants for different strains by HSE06+SOC method.

Strains δ	0%	4%	5.6%	6%	7%	8%	15%
Z_2	0	0	0	0	1	1	1

References

[1] P. E. Blochl, Phys. Rev. B: Condens. Mater. Phys. 1994, 50, 17953.
[2] G. Kresse and J. Furthmuller, Phys. Rev. B: Condens. Mater. Phys. 1996, 54, 11169.
[3] J. P. Perdew, L. Burke, and M. Ernzerhof, Phys. Rev. Lett. 1996, 77, 3865.
[4] H. Monkhorst, J. Pack, Phys. Rev. B: Condens. Matter 1976, 13, 5188.
[5] J. Heyd, G. E. Scuseria, and M. Ernzerhof, J. Chem. Phys. 2006, 124, 219906.
[6] A. Togo and I. Tanaka, Scr. Mater. 2015, 108, 1.
[7] G. J. Martyna, M. L. Klein, and M. Tuckerman, J. Chem. Phys. 1992, 97, 2635.
[8] S. J. Clark et al., Z. Kristallogr. - Cryst. Mater. 2005, 220, 567.
[9] Y. Wang, J. Lv, L. Zhu, and Y. Ma, Comput. Phys. Commun. 2012, 183, 2063.
[10] J. Bardeen and W. Shockley, Phys. Rev. 1950, 80, 72.
[11] M. Q. Long, L. Tang, D. Wang, L. Wang, and Z. G. Shuai, J. Am. Chem. Soc. 2009, 131, 17728.
[12] Q. S. Wu, S. N. Zhang, H. F. Song, M. Troyer, and A. A. Soluyanov, Comput. Phys. Commun.

2018, 224, 405.
[13] L. Zhou, Y. Zhang, and L. Wu, Nano Lett. 2013, 13, 5431.
[14] X. Luo, J. Yang, H. Liu, X. Wu, Y. Wang, Y. Ma, S. Wei, X. Gong, and H. Xiang, J. Am. Chem. Soc. 2011, 133, 16285.
[15] T. Yu, Z. Y. Zhao, Y. Sun, A. Bergara, J. Lin, S. Zhang, H. Xu, L. Zhang, G. Yang, and Y. Liu, J. Am. Chem. Soc. 2019, 141, 1599.